Chemical Engineering Journal 226 (2013) 189–200

Contents lists available at SciVerse ScienceDirect

Chemical Engineering Journal

journal homepage: www.elsevier.com/locate/cej

Simultaneous removal of Cd(II) and ionic dyes from aqueous solution using magnetic graphene oxide nanocomposite as an adsorbent

Jiu-Hua Deng, Xiu-Rong Zhang, Guang-Ming Zeng *, Ji-Lai Gong *, Qiu-Ya Niu, Jie Liang

College of Environmental Science and Engineering, Hunan University, Changsha 410082, PR China
Key Laboratory of Environmental Biology and Pollution Control, Ministry of Education, Hunan University, Changsha 410082, PR China

HIGHLIGHTS

- MGO was composed of iron oxide and graphene oxide.
- MGO simultaneously removes Cd(II) and ionic dyes including MB and OG.
- Synergistic adsorption for OG were obtained in Cd(II)–OG binary system.
- Suppression adsorption for Cd(II) were observed in Cd(II)–MB binary system.
- The tap water samples had little interference with the performance of MGO toward MB and OG.

ARTICLE INFO

Article history:
Received 28 January 2013
Received in revised form 8 April 2013
Accepted 10 April 2013
Available online 20 April 2013

Keywords:
Cd(II)
Ionic dyes
Magnetic graphene oxide
Simultaneous sorption

ABSTRACT

Heavy metal and ionic dyes commonly co-exist and constitute the most important and dangerous source of environmental pollution. Graphene oxide has the potential in the application to remove heavy metal ions and ionic dyes in wastewater, but it suffers from separation inconvenience. In this paper, magnetic graphene oxide (MGO) was synthesized and used as an adsorbent for simultaneous removal of Cd(II) and ionic dyes including methylene blue (MB) and orange G (OG). MGO adsorbent was characterized by transmission electron microscopy (TEM), scanning electron microscopy (SEM), X-ray powder diffraction (XRD) and X-ray photoelectron spectroscopy (XPS). The results showed that kinetic data followed a pseudo-second-order model and equilibrium data were well fitted by the Langmuir model. In mono-component system, the maximum sorption capacities in ultrapure water for Cd(II), MB and OG were 91.29 mg/g, 64.23 mg/g and 20.85 mg/g, respectively. The sorption capacity suppressed for Cd(II) with increasing MB concentration and almost was not affected for MB with increasing Cd(II) concentration in Cd(II)–MB binary system. However, the sorption capacity enhanced for OG with increasing Cd(II) concentration and for Cd(II) was independent on the concentration of OG in Cd(II)–OG binary system. In tap water samples, the sorption capacity for Cd(II) was 65.39% of that in ultrapure water. However, the tap water samples had little interference with the performance of MGO toward MB and OG, indicating that MGO was suitable for removal of ionic dyes from real water.

1. Introduction

Ionic dyes discharged from the textile, printing, and tanning industries commonly are toxic, and some are carcinogenic and mutagenic, causing deterioration in water quality, influencing the photosynthetic activity of aquatic organism [1]. Cadmium is one of the most toxic heavy metals to environment and human beings due to its detrimental effects on the environment and human health [2]. Many diseases, such as renal damage, emphysema, hypertension, cardiovascular disorder, diabetes mellitus, and skeletal malformation, are related to cadmium [3]. Recently, ionic dyes and heavy metal ions commonly co-exist and constitute the most important and dangerous source of environmental pollution [1]. Therefore, it is urgent to find an efficient and cost-effective method to simultaneously remove these co-pollutions.

Sorption, which is easy to perform, insensitive to toxic substance, is considered as a fast and relatively inexpensive approach for wastewater treatment [4]. Many materials were used as adsorbents, such as activated carbon, agricultural and industrial residues, TiO_2, chitosan-coated quartz sand, modified mesoporous silica, montmorillonite, and kaolinite [5–10]. Tovar-Gomez et al. reported synergic adsorption in the simultaneous removal of acid

* Corresponding authors at: College of Environmental Science and Engineering, Hunan University, Changsha 410082, PR China. Tel./fax: +86 731 88823701.
E-mail addresses: zgming@hnu.edu.cn (G.-M. Zeng), jilaigong@gmail.com (J.-L. Gong).

1385-8947/$ - see front matter © 2013 Elsevier B.V. All rights reserved.
http://dx.doi.org/10.1016/j.cej.2013.04.045

blue 25 and heavy metals using a $Ca(PO_3)_2$-modified carbon [11]. Shukla and Pai investigated adsorption of copper, nickel and zinc ions on dye loaded groundnut shells and sawdust [12]. Visa et al. reported simultaneous adsorption of dyes and heavy metals from multi-component solutions using fly ash [13]. Noticeably, carbonaceous adsorbents such as granular activated carbon, activated carbon fiber, carbon nanotubes have attracted attention of many scientists in the past several decades due to their availability, low-cost, stability and high sorption capacities. Chen et al. investigated europium adsorption on multiwall carbon nanotube/iron oxide magnetic composite in the presence of polyacrylic acid [14]. Zaini et al. prepared activated carbon derived from polyacrylonitrile fiber for removal of heavy metals Cu(II) and Pb(II) [15]. Zhou et al. reported ferric oxide doped activated carbon fiber for phosphorous removal from contaminated waters [16]. Yang et al. investigated mutual effects of Pb(II) and humic acid adsorption on multi-walled carbon nanotubes/polyacrylamide composites from aqueous solution [17]. Our group also reported simultaneous sorption of atrazine and Cu(II) from wastewater by magnetic multi-walled carbon nanotube [18]. Zhang et al. compared the adsorption properties of three aromatic organic compounds on four types of carbonaceous adsorbents including granular activated carbon, activated carbon fiber, single-walled carbon nanotubes and multi-walled carbon nanotube, with different structural characteristics but similar surface polarities [19]. They demonstrated that molecular sieving and micropore effects were very important in the adsorption of (AOCs) by carbonaceous porous adsorbents [19].

Graphene, a single or several atomic layered graphites, is a fascinating new class of two-dimensional carbon nanostructure and possesses excellent mechanical, thermal and electrical properties [20]. It has showed great promise in the application of electronic devices, solar cells, sensors, batteries, supercapacitors, hydrogen storage and environmental pollution remediation [21,22]. Graphene exhibits huge surface area with a calculated value of 2630 m^2/g, good chemical stability and graphitized basal plane structure, thus providing strong π–π interactions with the aromatic moieties present in many dyes [23]. However, graphene itself is hydrophobic substance, thus preventing it as an adsorbent for directly removing dye pollutants from aqueous solution. Graphene oxide (GO), the oxidation product of graphene containing hydroxyl, epoxide, carboxyl and carbonyl functional groups, is hydrophilic, negatively charged, and readily disperses in aqueous solution to form a stable suspension [24,25]. Therefore, GO has the potential in the application to remove ionic dyes and heavy metal ions in wastewater [20,25–27]. However, carbonaceous adsorbents described above suffered from separation inconvenience. Due to the high separation convenience, magnetic nanoparticles have been widely used in environment remediation [28]. It was believed that magnetic graphene oxide (MGO), exhibiting high sorption and easy separation properties, would have better performances in water purification. Recently, a few researchers focused on MGO adsorbents for removing dyes [21,23,29,30] or heavy metal ions [4,31–33]. However, to our knowledge, there is no prior report on simultaneous removal of dyes and heavy metal ions using MGO as an adsorbent.

In this paper, MGO nanocomposite was synthesized and was used as an adsorbent for simultaneous removal of ionic dyes and Cd(II). MGO nanocomposite was characterized by scanning electron microscopy (SEM), transmission electron microscopy (TEM), X-ray diffraction (XRD) and X-ray photoelectron spectroscopy

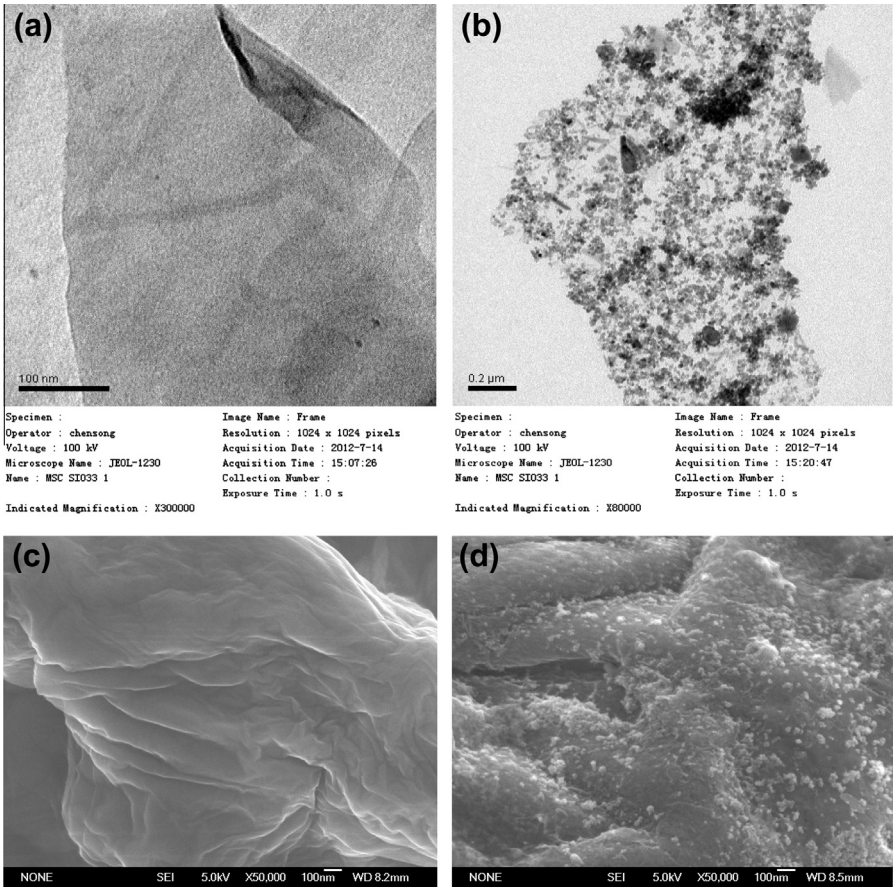

Fig. 1. TEM and SEM images of GO and MGO nanomaterials. (a) TEM of GO, (b) TEM of MGO, (c) SEM of GO and (d) SEM of MGO.

(XPS). Methylene blue (MB) and orange G (OG) were chosen as model cationic and anionic dyes, respectively. Multi-component sorption behaviors were also investigated using binary systems including Cd(II)–MB and Cd(II)–OG. The different removal performance of MGO toward ionic dyes and Cd(II) in ultrapure water and in tap water was investigated. Other experimental parameters such as effects of contact time and pH on removal performance were also investigated.

2. Materials and methods

2.1. Materials

MB, OG, Ferrous ammonium sulfate [$(NH_4)_2SO_4{\cdot}FeSO_4{\cdot}6H_2O$] and ammonium ferric sulfate [$NH_4Fe(SO_4)_2{\cdot}12H_2O$] were purchased from Sinopharm chemical reagent Co., (Shanghai, China). $Cd(NO_3)_2$ standard sample was purchased from Institute for Environmental Protection in China. Graphite powder was purchased from Shanghai JinShanTing new chemical factory (Shanghai, China). All regents used were of analytical grade. Ultrapure water was used in all the experiments.

2.2. Synthesis of GO

The synthesis of GO was performed by natural graphite powder oxidation according to the Hummer and offeman's method [34]. Briefly, 1 g of graphite powder and 0.5 g of $NaNO_3$ were sequentially added into cold 98% H_2SO_4 under the condition of ice bath, followed by slow addition of 3 g $KMnO_4$ with stirring at the temperature below 20 °C. Subsequently, the reaction was continued for 30 min at 35 °C, followed by slow addition of 46 mL ultrapure water under stirring. The reaction was continued for 15 min at 98 °C. Then, the mixture was diluted to 140 mL with subsequent addition of 2.5 mL H_2O_2 (wt. 30%). The resulting mixture was filtered and was washed three times with ultrapure water and alcohol, respectively, and then dried at 70 °C for 12 h in vacuum oven.

2.3. Synthesis of MGO

The preparation of iron oxide magnetic nanoparticle was performed by coprecipitation of iron oxide nanoparticles on the surface of GO nanomaterials. Typically, 1 g dry GO was dispersed in 100 mL ultrapure water with ultrasonication to form stable suspension. Then, 5.8 g ferrous ammonium sulfate and 10.7 g ammonium ferric sulfate were dissolved in 100 mL ultrapure water to form mixed iron salt solution under oxygen-free condition. Subsequently, 10 mL aqueous ammonia (wt. 25%) was rapidly added into the mixed solution to produce iron oxide nanoparticles, followed by slow addition of GO suspension with stirring. The reaction was continued for 45 min at 85 °C with stirring for 45 min and then cooled to room temperature. Finally, the MGO solid was collected by a magnet and was washed with ultrapure water and anhydrous ethanol three times, respectively, and dried at 70 °C for 12 h in vacuum oven.

2.4. Characterization of adsorbent

The morphologies of GO and MGO were observed by scanning electron microscopy (SEM) (JSM-6700F LV microscope) and transmission electron microscopy (TEM) (JEOL-1230 microscope, Japan). The structural information was obtained by X-ray diffraction (XRD) (D/max 2550 X-ray diffractometer, RigaKu, Japan). The composition and bond energy information of MGO itself and MGO loaded with dyes and Cd(II) were investigated by X-ray photoelectron spectroscopy (XPS) (K-Alpha 1063, United Kingdom) using a Thermo Fisher Scientific Theta Probe Spectrometer equipped with Al Kα Micro gathered monochromator as the source of X-ray. XPS measurements were performed using a monochromatic 400 μm X-ray beam in constant analyser energy mode. Survey and high-resolution spectra were obtained at a pass energy of 200 and 50 eV, respectively and with a step size of 1.0 and 0.1 eV, respectively. Detailed spectra processing was performed by commercial *Thermo Avantage* software (v. 4.75, © 1999–2010 Thermo Fisher Scientific). Accurate curve-fitting analysis was applied to the high-resolution spectra of C1s, O1s and Fe2p using a Smart type background and Gaussian/orentzian peak shapes. Calibration of the binding energy (BE) scale was obtained by fixing the aliphatic

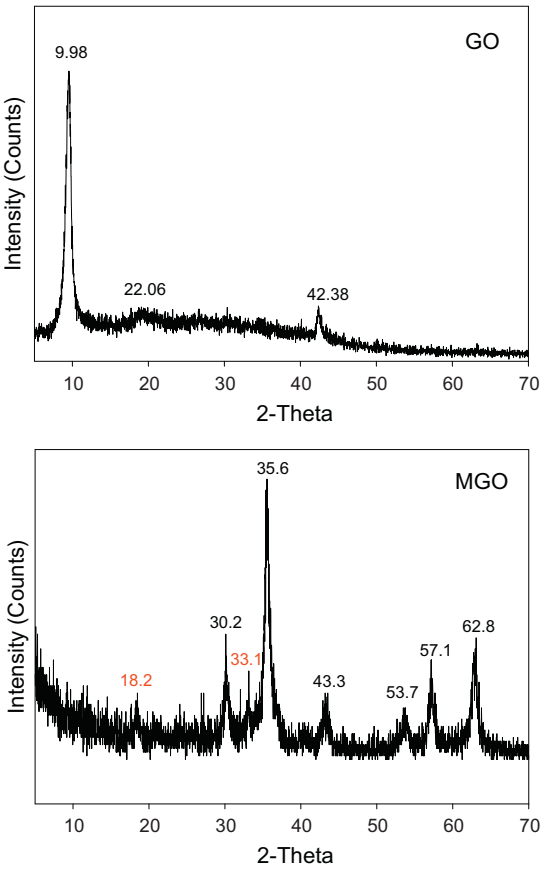

Fig. 2. XRD patterns of the GO and MGO.

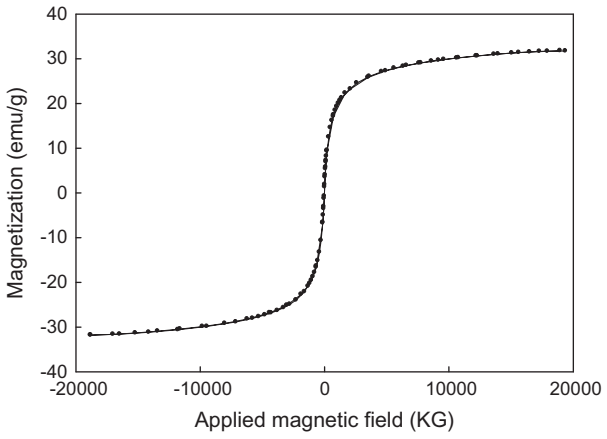

Fig. 3. Magnetization curve of MGO nanocomposite.

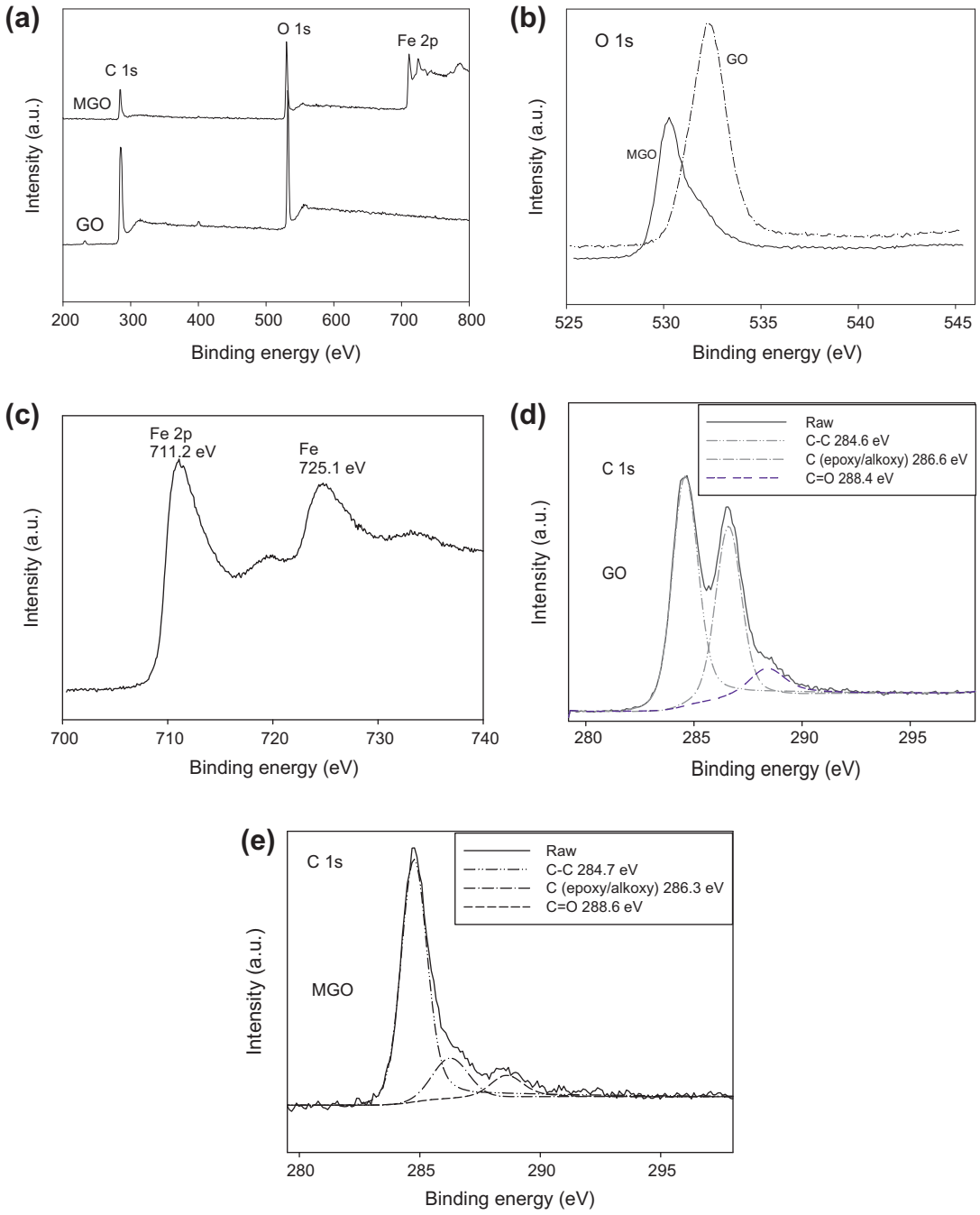

Fig. 4. XPS spectra of GO and MGO. (a) Wide scan, (b) O 1s spectra, (c) Fe 2p spectrum of MGO, (d) C 1s spectra of GO and (e) C 1s spectra of MGO.

C1s component at BE values of 284.8 ± 0.1 eV. The base pressure was below 5×10^{-9} mbar. Magnetization curve was recorded on a Lake Shore 7410 vibrating sample magnetometer. The zeta potential of adsorbent was obtained using a Zeta Meter 3.0 (Zeta Meter Inc.).

2.5. Sorption experiments

All sorption experiments were performed by adding 20 mg MGO adsorbent into 20 ml metal solution and dye solutions with different concentrations at specified pH value which was adjusted using 0.1 M NaOH and HCl. After sorption, MGO adsorbent was separated from aqueous solution by a permanent magnet. The residual concentrations of Cd(II) and dyes were measured using atomic absorption spectroscopy and the visible spectrophotometric method at the maximum sorption wavelength (λ_{max}: 667 nm for MB and 475 nm for OG, respectively). All the measurements were carried out in duplicate.

Table 1
Results of XPS analysis of GO and MGO before and after the uptake of Cd(II), MB and OG.

Elements	at.% In adsorbent sample				
	GO	MGO	MB–MGO	OG–MGO	Cd–MGO
C	66.58	37.30	40.78	35.52	40.53
N	2.16	1.40	2.20	0.94	
O	28.78	41.00	38.40	41.97	41.06
Fe		20.30	17.40	20.36	18.19
Cd					0.22
S	2.27		1.21	1.22	
Ca	0.22				

2.5.1. Effect of pH

The effect of pH on sorption of MGO toward Cd(II) and dyes was investigated by mixing 20 mg MGO with 20 mL of 200 mg/L Cd(II), or 20 ml of 90 mg/L MB or 20 mL of 60 mg/L OG at different initial pH values under stirring for 24 h. For dyes, the initial pH values varied between 3 and 10, but for Cd(II), the initial pH values ranged from 3 to 8. After magnetic separation, the concentrations of Cd(II) and dyes were measured.

2.5.2. Sorption kinetic experiments

Kinetic experiments were carried out by mixing 20 mg MGO with 20 mL of 200 mg/L Cd(II), or 20 mL of 90 mg/L MB, or 20 mL of 60 mg/L OG aqueous solutions in conical flasks at pH 6.0. The samples were withdrawn at predetermined time 5 min, 25 min, 45 min, 1 h 45 min, 2 h 45 min, 4 h 45 min, 6 h 45 min, 10 h 45 min, 24 h, 36 h, 48 h. After magnetic separation, the residual concentrations of Cd(II) and dyes were measured. The sorption quantity at any time was calculated according to the following equation:

$$q_t = \frac{(c_0 - c_t)V}{m} \quad (1)$$

where q_t is sorption quantity, c_0 and c_t are the initial and residual concentrations of the analyte, respectively, V is the volume of analyte solution and m is the mass of MGO adsorbent.

2.5.3. Isothermal sorption

Isothermal sorption experiments included single-component and multi-component sorption (i.e. binary system). (a) For single-component system, sorption experiments were conducted at pH 6.0 for 24 h under stirring by mixing 20 mg MGO with 20 mL solutions with known initial concentrations ranging from 10 mg/L to 120 mg/L for MB, from 10 mg/L to 150 mg/L for OG, and from 10 mg/L to 1000 mg/L for Cd(II), respectively, with subsequent magnetic separation and the analysis of residual concentrations of dyes or Cd(II). (b) For multi-component system, binary sorption experiments including Cd(II)–MB and Cd(II)–OG were conducted by mixing 20 mg MGO with 20 mL analyte solutions containing both dyes and Cd(II) at pH 6 for 24 h under stirring. For Cd(II)–MB binary system, the initial concentrations of Cd(II) and MB were from 10 to 300 mg/L and from 30 to 120 mg/L, respectively. For Cd(II)–OG binary system, the initial concentrations of Cd(II) and OG were from 10 to 300 mg/L and from 20 to 120 mg/L, respectively. After sorption and magnetic separation, the residual analyte concentrations including both dyes and Cd(II) were determined.

2.5.4. Desorption and reusability

The desorption and the reusability of MGO adsorbent were investigated using HCl solution (pH = 3) for Cd(II) and ethylene glycol (EG) for MB and OG as effluent solutions. Typically, the MGO adsorbent was first saturated with Cd(II), MB and OG for 24 h with the initial concentrations of 500, 120 and 150 mg/L for Cd(II), MB and OG, respectively. The adsorbent dosage was 1 g/L. Then MGO was separated from the solution by a magnet and was subsequently immersed in HCl solution (pH 3) for Cd(II) and in ethylene glycol (EG) for MB and OG for another 24 h at room temperature. After reaction and subsequent magnetic separation, the remaining adsorbates in supernatant including Cd(II), MB and OG were measured.

2.5.5. Removal performance of MGO in tap water

To investigate MGO adsorbent performance in real sample, the sorption experiments were performed in tap water. Supporting information (SI) Table S1 summarizes the chemical analysis of the tap water. Typically, 20 mg MGO was mixed with 20 mL of known concentration of analyte solutions prepared by adding MB, OG and cadmium nitrate to the tap water samples. Then 1 g/L of MGO was added in the tap waters at pH 6.0 and the removal efficiencies were investigated. The sorption process was continued for 24 h under stirring. After magnetic separation, the final concentrations of dyes and Cd(II) were determined, respectively.

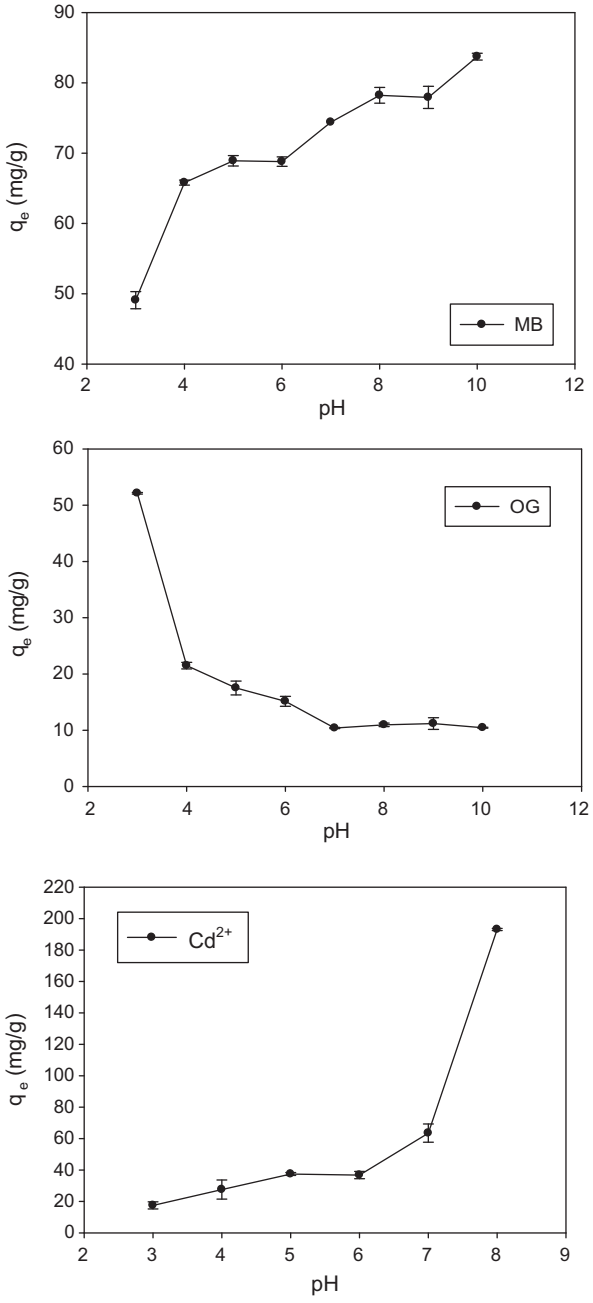

Fig. 5. pH effects on MGO sorption toward MB, OG and Cd(II).

3. Results and discussion

3.1. Characterization

As seen from Fig. 1, GO exhibited layered structure with smooth surface and many wrinkles (Fig. 1a and c). For MGO, it was observed that many nanoparticles with an average size of 10.8 ± 1.7 nm were homogeneously anchored onto the surface of

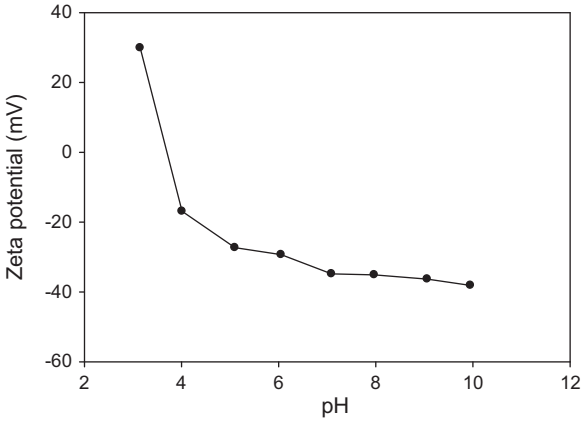

Fig. 6. Zeta potentials of MGO at various pH values.

the graphene oxide sheets (Fig. 1b, d and Fig. S1 in the Supporting information).

In the XRD patterns (Fig. 2) of GO nanosheet and MGO nanocomposite, the diffraction peak at $2\theta = 9.98°$, corresponding to the typical diffraction peak of GO nanosheets, was attributed to the (002) plane [20]. Two weak peaks at $2\theta = 22.06°$ and 42.38° also occur, which were similar to typical GO XRD patterns in previous literature [24]. For MGO, the peaks at 2θ values of 30.2°, 35.6°, 43.3°, 53.7°, 57.1°, and 62.8° were assigned to the (220), (331), (400), (422), (511), and (440) reflections, respectively, of the pure cubic spinel crystal structure of Fe_3O_4 [23]. Furthermore, the peaks at 2θ values of 30.2°, 35.6°, 43.3° and 57.1° were assigned to maghemite or magnetite, and the peaks at $2\theta = 53.7°$ and 62.8° were attributed to hematite [35]. The peaks at $2\theta = 18.2°$ and 33.1° were assigned to goethite [36]. Noticeably, GO peak disappeared in XRD pattern of MGO (Fig. 2). This phenomenon was also observed by Wang's group [37]. They considered that the disappearance of GO peak in XRD pattern of MGO may be derived from the following reasons: (1) more monolayer graphene caused by the reduction of graphene sheets aggregation in the presence of magnetite, resulting in weaker peaks from carbon being observed; (2) the strong signals of the iron oxides overwhelming the weak carbon peaks [37]. The measured saturation magnetization of MGO adsorbent was 31.8 emu/g (see Fig. 3), which was strong enough to separate from aqueous solution because saturation magnetization of 16.3 emu/g was sufficient for magnetic separation with a conventional magnet [38].

Fig. 4 shows the XPS analysis in GO and MGO nanomaterials. Compared to GO, the new peaks of Fe 2p appeared in MGO adsorbent (Fig. 4a), further illustrating iron oxide nanoparticles were successfully coated on GO nanosheet. The binding energies of Fe $2p_{3/2}$ and Fe $2p_{1/2}$ were 711.2 eV and 725.1 eV, respectively. The satellite peak of Fe $2p_{3/2}$ for MGO was located at 719.4 eV, which was consistent with the previous report (Fig. 4c) [32,39]. The binding energy assigned to O 1s shifted from 532.3 eV in GO to 530.3 eV in MGO, which was characteristic of the lattice oxygen in magnetite (Fig. 4b) [23,33]. The deconvolution C 1s XPS spectra (Fig. 4d and e) showed that the nonoxygenated ring C, located at 284.6 eV in GO and 284.7 eV in MGO, was 53.47 at.% and 74.11 at.% in GO and MGO respectively, providing the evidence of the formation of graphene in MGO compared with that in GO [23]. The peaks assigned to C (epoxy and alkoxy) were observed at 286.6 eV, 37.40 at.% in GO and 286.3 eV, 16.45 at.% in MGO, indicating the decrease of the oxygen-containing functional groups after GO coated with iron oxide nanoparticles [23,33]. The peaks assigned to C=O were located at 288.4 eV, 9.14 at.% in GO and 288.6 eV, 9.44 at.% in MGO, illustrating the little increase of carbonyl groups in MGO compared with that in GO. Compared with the XPS spectrum of MGO, 1.21 at.% of S and 1.22 at.% of S

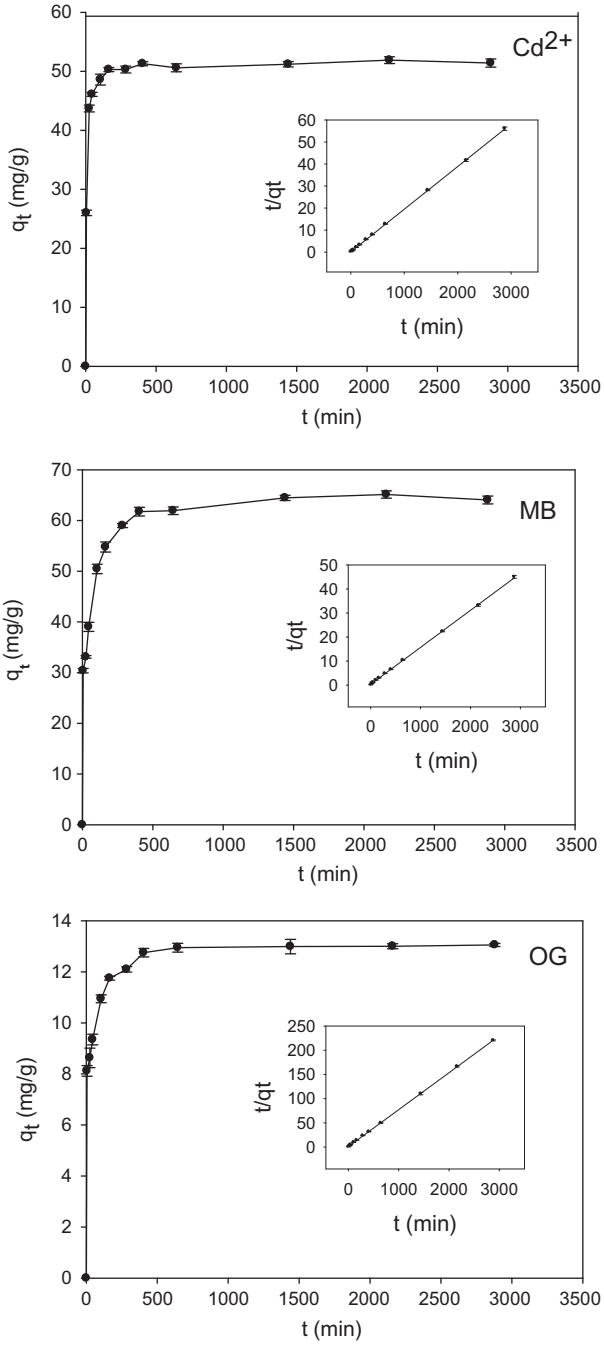

Fig. 7. Influence of contact time on the sorption of Cd(II), MB and OG by MGO. Inserted part: the plots of t/q_t *vs.* t. The initial concentrations were 200 mg/L, 90 mg/L and 60 mg/L for Cd(II), MB and OG, respectively; pH = 6; contact time: 5 min, 25 min, 45 min, 1h45 min, 2h45 min, 4h45 min, 6h45 min, 10h45 min, 24 h, 36 h and 48 h; temperature: 25 °C; adsorbent dosage: 1 g/L.

Table 2
Parameters of adsorption kinetics of Cd(II), MB and OG onto MGO fitted by pseudo-second-order model.

Pollutants	q_e (mg/g)	k (g/mg min)	R^2
Cd(II)	51.55	0.1971	0.9998
MB	64.94	0.0389	0.9996
OG	13.12	0.3175	0.9998

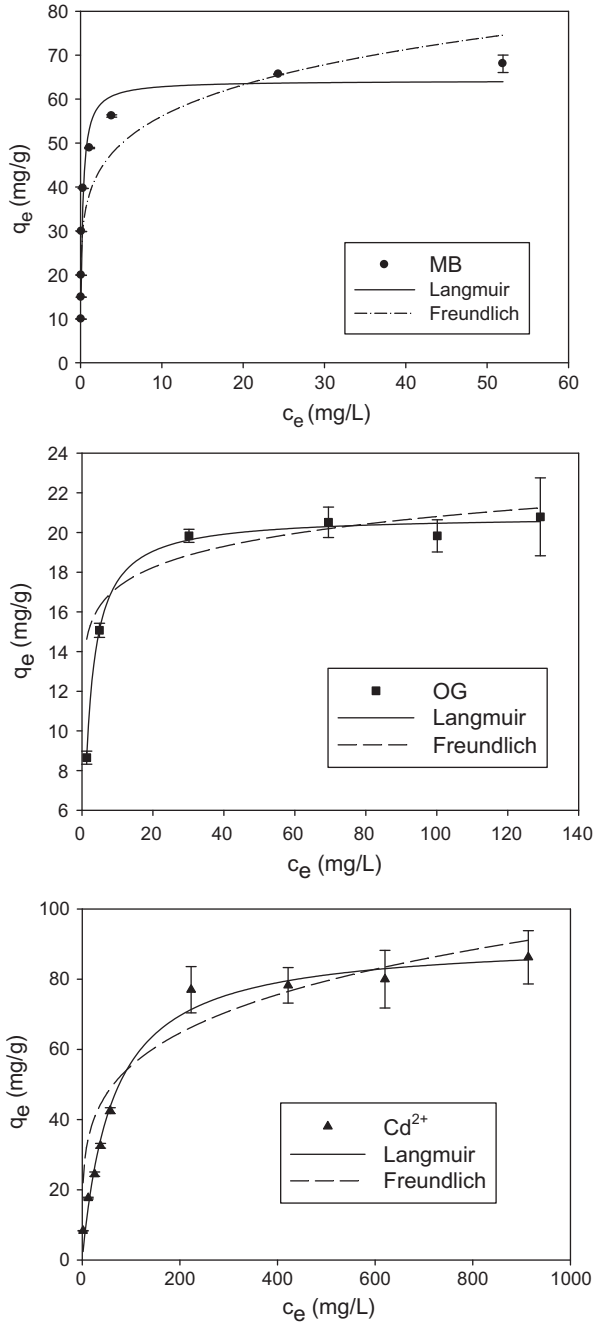

Fig. 8. Sorption isotherms of MB, OG and Cd(II) on the MGO, fitted by Langmuir and Freundlich models. pH = 6; contact time: 24 h; temperature, 25 °C; adsorbent dosage, 1 g/L.

appeared in MGO after MB and OG uptake by MGO (see Fig. S2 and Table 1) indicated that MB and OG adsorbed on MGO, respectively. In addition, Cd 3d peaks (0.22 at.% shown in Table 1) at 412.48 eV and 405.77 eV (Fig. S2) as an indicator of Cd(II) sorption on MGO were detected [40], which provided the evidence that Cd(II) were successfully adsorbed onto MGO. Table 1 lists the XPS results of GO and MGO adsorbent before and after MGO uptake by dyes and Cd(II).

3.2. Effect of pH

The influence of pH on dyes removal efficiencies by MGO adsorbent at different pH values was studied and the results were shown in Fig. 5. It was observed that the quantity of MB and Cd(II) adsorbed onto MGO increased with increasing pH value. Similar results were obtained for Cd(II) sorption on crosslinked carboxymethyl starch [41] and magnetic hydroxyapatite nanoparticles [42]. Noticeably, the pH values ranged from 3 to 8 due to the formation of $Cd(OH)_2$ precipitation at pH greater than 8 [42]. It was observed that the pH_{PZC} value of MGO was approximately 3.5. The surface charge was positive at pH < 3.5, but was negative at pH > 3.5. Furthermore, the zeta potentials of MGO adsorbent decreased with increasing pH value (shown in Fig. 6). Therefore, the effect of pH on Cd(II), MB and OG adsorption onto MGO can be explained by electrostatic interaction mechanism between MGO surface and charged adsorbates. Due to electrostatic attraction force, MGO adsorbent with negative charge surface at higher pH (>3.5) value favored sorption toward cationic dye MB and Cd(II) with positive charge. In contrast, for anionic dye OG, the sorption quantity decreased with increasing pH value due to electrostatic repulsion force.

3.3. Sorption kinetics

The effect of contact time on sorption of Cd(II), MB and OG onto MGO adsorbent was carried out and the results were displayed in Fig. 7. Obviously, sorption capacity increased sharply with time and the time required to reach the equilibrium was 165 min, 405 min and 405 min for Cd(II), MB and OG respectively. Benselka-Hadj Abdelkader et al. reported that sorption equilibrium of OG was reached after 12 h and 9 h on layered double hydroxide and calcinated layered double hydroxide, respectively [43]. Han et al. reported methylene blue sorption onto natural zeolite to reach equilibrium after 820 min [44]. Liu et al. reported that 855 min was required to reach equilibrium for initial concentration of 40 mg/L MB adsorbed on graphene [45]. According to the results of the experiments, 24 h was selected in this study for the following sorption equilibrium study.

The kinetic data were fitted with pseudo-second-order kinetic model, the relationship between sorption quantity and time can be described with the following equation:

Table 3
Constants of the Langmuir and Freundlich models for Cd(II), MB and OG in ultrapure water and tap water at pH 6.0.

Pollutants		Langmuir model			Freundlich model		
		q_m (mg/g)	k_L (l/mg)	R^2	k_f	$1/n$	R^2
Cd(II)	Ultrapure water	91.29	0.0160	0.9688	19.5655	0.2256	0.9001
	Tap water	59.69	0.2097	0.9568	24.0296	0.1651	0.7031
MB	Ultrapure water	64.23	4.4344	0.9603	37.7252	0.1725	0.8356
	Tap water	58.08	2.2528	0.9549	29.8169	0.1922	0.9268
OG	Ultrapure water	20.85	0.5301	0.9589	14.2659	0.0819	0.7671
	Tap water	20.48	0.7372	0.9614	10.7478	0.1688	0.9242

Table 4
Comparison of the maximum adsorption capacities of some adsorbents for MB, OG and Cd(II).

Pollutants	Adsorbents	q_{max} (mg/g)	References
MB	Magnetic rectorite/iron oxide	31.18	[47]
	Graphene nanosheet/magnetite	43.82	[48]
	Multi-walled carbon nanotubes/Fe_2O_3	42.30	[49]
OG	Activated carbon of thespesia populnea pods	9.13	[50]
Cd(II)	Acrylic acid and crotonic acid modified magneti nanoparticles	29.60	[51]
	$CuFe_2O_4$ nano-particles	17.54	[52]
	Carbon nanotube sheets	92.59	[53]

$$\frac{t}{q_t} = \frac{1}{kq_e^2} + \frac{t}{q_e} \tag{2}$$

where q_t and q_e is sorption quantity at time t and at equilibrium, respectively, c_0 and c_t are the initial concentration and the final concentration at time t of the analyte, respectively, k is the rate constant, which can be calculated from the plot of t/q_t *vs.* t.

The results of linear forms of pseudo-second-order kinetic model on the experiment data were presented in Fig. 7 (inserted part). Table 2 lists the kinetic parameters for the removal of Cd(II), MB and OG by MGO adsorbent using pseudo-second-order model. A linear relationship with high correlation coefficient (R^2 = 0.9998, 0.9996 and 0.9998 for Cd(II), MB and OG, respectively) was obtained, illustrating that the kinetic data were well fitted with the pseudo-second-order model.

3.4. Sorption isotherms

3.4.1. Sorption isotherms in mono-component system

Two different sorption isotherms, i.e. Langmuir and Freundich models, were used to fit the experimental sorption data for MB, OG and Cd(II). The Langmuir model is based on monolayer sorption and can be described as the following equation:

$$\frac{c_e}{q_e} = \frac{c_e}{q_m} + \frac{1}{k_L q_m} \tag{3}$$

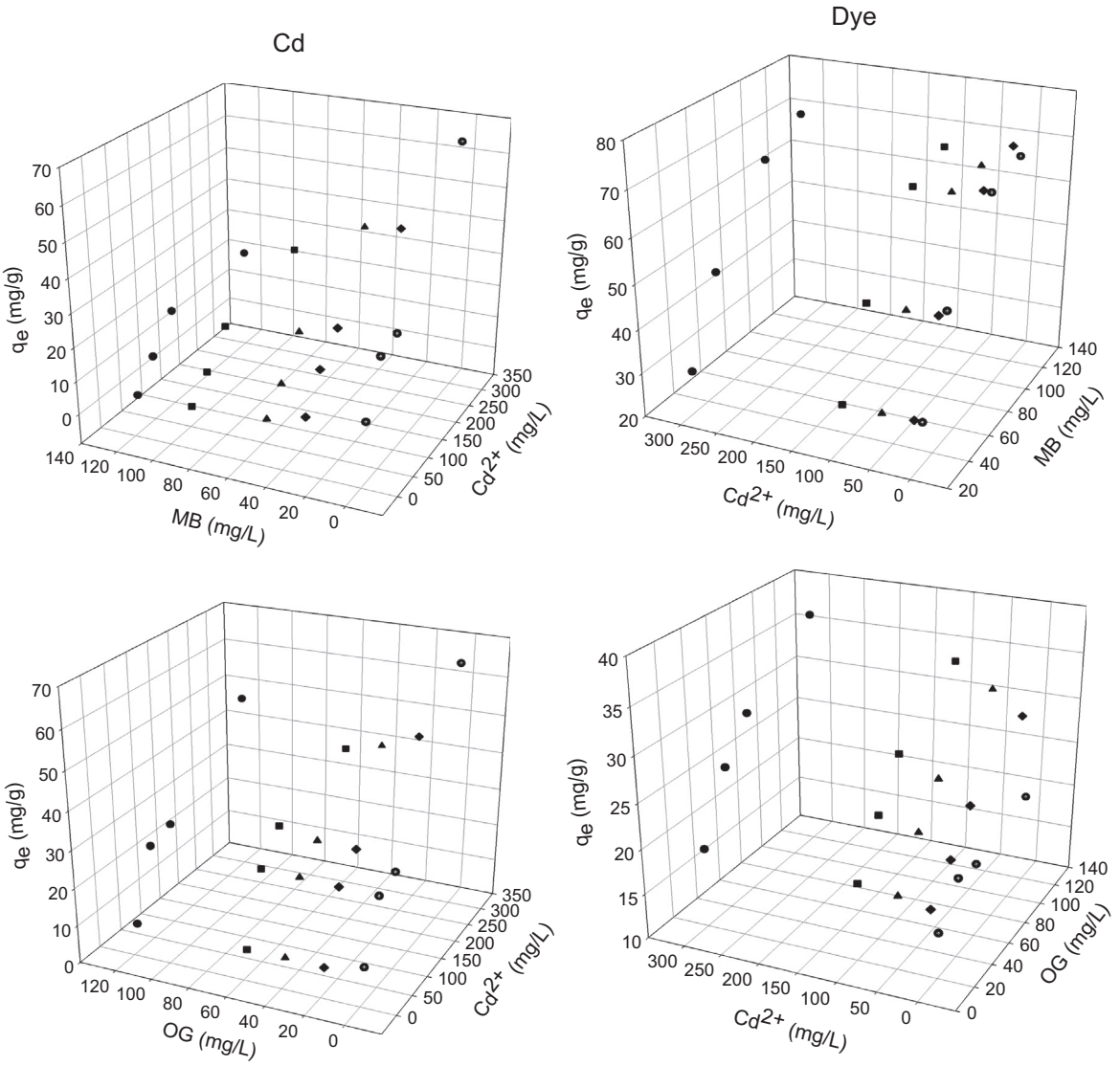

Fig. 9. Effect of initial pollutant concentration on the sorption of Cd(II), MB and OG onto MGO in binary system including Cd(II)–MB and Cd(II)–OG. The initial concentrations: for Cd(II), 10 mg/L, 50 mg/L, 100 mg/L and 300 mg/L; for MB, 30 mg/L, 50 mg/L, 90 mg/L and 120 mg/L; for OG, 20 mg/L, 40 mg/L, 60 mg/L, and 120 mg/L; pH = 6, contact time: 24 h; temperature, 25 °C; adsorbent dosage, 1 g/L.

The Freundlich model is based on multilayer sorption and is given by the following equation:

$$\lg q_e = \lg k_f + \frac{1}{n}\lg c_e \quad (4)$$

where q_e is the equilibrium sorption amount of dyes or Cd(II) adsorbed on MGO (mg/g), q_m is the maximum sorption amount of MGO (mg/g), c_e is the equilibrium concentration of adsorbates in aqueous solution (mg/L), k_L is a constant determined by plotting c_e/q_e versus c_e, k_f and $1/n$ are the constants related to sorption of adsorbent and intensity of the sorption, respectively.

Fig. 8 shows that the sorption isotherms data of dyes and Cd(II) were better fitted with Langmuir model in mono-component system. The calculated isotherm constants and correlation coefficients of Langmuir and Freundlich models were listed in Table 3. The sorption capacities of adsorbates on MGO were 64.23 mg/g, 20.85 mg/g and 91.29 mg/g for MB, OG and Cd(II), respectively. It was noted that the maximum sorption capacities of MGO toward MB (64.23 mg/g) and OG (20.85 mg/g) were much higher than previous reported adsorbents, such as exfoliated graphene oxide (17.3 mg/g for MB and 5.98 for OG) [46]. Table 4 summarizes the maximum sorption capacities of various absorbents for MB, OG and Cd(II). It was observed that the amount of dyes and Cd(II) adsorbed by bare iron oxide nanoparticles were 2.78, 15.62 and 24.25 mg/g for MB, OG and Cd(II), respectively. Therefore, the adsorption of MGO toward Cd(II) and ionic dyes not only resulted from iron oxide nanoparticles but also from graphene oxide. The high-performance of the MGO adsorbent towards ionic dyes may be ascribed to the π–π stacking between dyes with aromatic structure of MB and OG and π-conjugation regions of the MGO nanosheets (see Fig. S3) [21,29,46]. On the other hand, according to the results described above, the electrostatic interactions between the positively charged adsorbates (i.e. MB and Cd(II)) and negatively charged residual oxygen-containing functional groups on MGO may also play an important role in the sorption of MGO toward MB and Cd(II).

3.4.2. Effect of initial pollutant concentration in multi-component system

The effects of the initial pollutant concentrations on the sorption of Cd(II) and dyes onto MGO were investigated in binary system (see Fig. 9). Results showed that the sorption of Cd(II) onto MGO decreased in the presence of MB (Fig. 9). Furthermore, the sorption capacity of Cd(II) decreased with increasing concentration of MB (Fig. 9). At the initial Cd(II) concentration of 300 mg/L, the

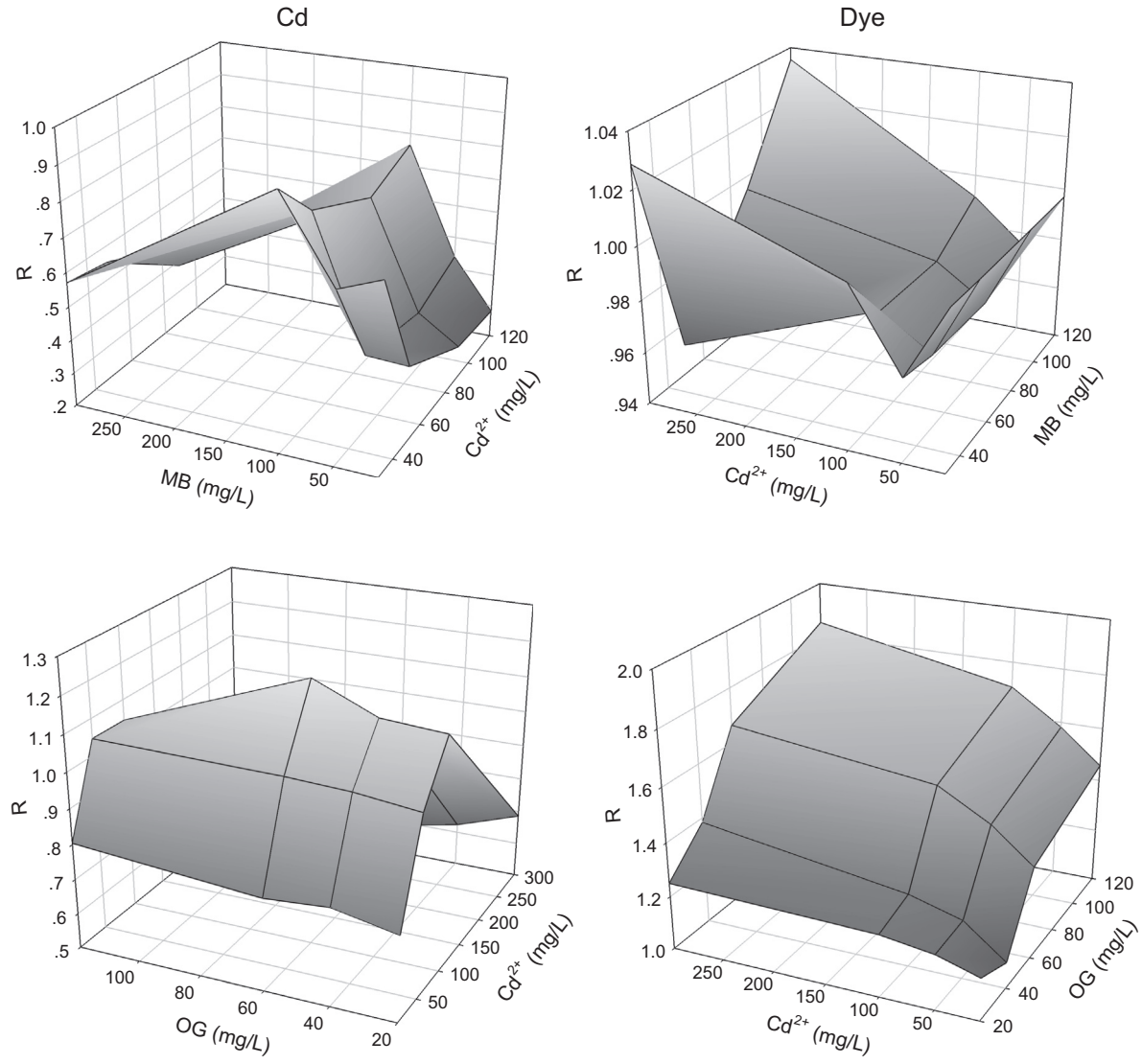

Fig. 10. Ratio of sorption capacities (R) versus the initial concentration in binary system for the simultaneous removal of Cd(II), MB and OG using MGO adsorbent.

sorption capacity for Cd(II) was 65.25 mg/g in mono-component system and 21.38 mg/g in Cd(II)–MB binary system at the initial MB concentration of 120 mg/L. i.e., the sorption capacity of Cd(II) in Cd(II)–MB binary solutions was only 32.76% of that in mono-component system. However, the sorption of MB onto MGO were not affected by the presence of Cd(II) in Cd(II)–MB binary solutions. The sorption capacity of Cd(II) was independent on the OG concentration, but dependent on the initial Cd(II) concentration in Cd(II)–OG binary system. Noticeably, the sorption capacity of OG onto MGO enhanced with increasing Cd(II) concentration in Cd(II)–OG binary system.

The effect of both Cd(II) and ionic dyes in binary system on removal performance of MGO were determined using the ratio of sorption capacities (R) as follows:

$$R = \frac{q_{b,i}}{q_{m,i}} \tag{5}$$

where $q_{b,i}$ is the sorption quantity for contaminant i in the binary system (mg/g) and $q_{m,i}$ is the sorption quantity for contaminant i with the same initial concentration in a mono-component system. It was reported that [11]: if $R > 1$, the sorption of contaminant i was enhanced by the co-pollutant; if $R = 1$, the co-pollutant had no effect on the sorption of contaminant i; if $R < 1$, the sorption of contaminant i was suppressed by the presence of co-pollutant.

Fig. 10 shows that R value was less than 1 for sorption of Cd(II) onto MGO in Cd(II)–MB binary system, which may be caused by the following reasons: (1) competitive sorption between positively charged Cd(II) and positively charged MB, (2) favorable sorption of MB due to π–π interaction between MB and MGO nanosheets compared with that of Cd(II) due to electrostatic force. However, R value was almost equal to 1 for MB sorption in Cd(II)–MB binary system, thus discarding the competitive sorption between positively charged Cd(II) and positively charged MB. It revealed that sorption of MB was favored in comparison with that of Cd(II) in Cd(II)–MB binary system. Noticeably, R value was greater than 1 for OG sorption in Cd(II)–OG binary system, indicating that sorption of OG onto MGO was favored due to π–π interaction between OG and MGO in Cd(II)–OG binary system. Furthermore, OG sorption was greatly enhanced in the presence of Cd(II). The reason may be caused by the fact that anionic dye OG adsorbed on the surface of MGO favored the electrostatic interactions with Cd(II), thus creating new specific sites for sorption process and enhancing the sorption capacity of OG onto MGO. Heavy metal Cd(II) may interact with the SO_3^- group of OG and with the hydroxyl and carboxyl groups of MGO. Synergic sorption was also reported by Tovar-Gomez et al. for the simultaneous removal of acid blue 25 and heavy metals from water using a $Ca(PO_3)_2$-modified carbon [11]. However, the sorption of Cd(II) decreased at the initial Cd(II) concentration of 10 mg/L ($R < 1$), remained stable at the initial Cd(II) concentration of 50 mg/L ($R \approx 1$), slightly increased at the initial Cd(II) concentration of 100 mg/L ($R > 1$), and then decreased at the initial Cd(II) concentration of 300 mg/L ($R < 1$). It was suggested that OG was preferentially adsorbed onto MGO surface at the initial Cd(II) concentration of 10 mg/L, leading to the decrease of Cd(II) sorption capacity in Cd(II)–OG binary system. Increasing OG concentration on the surface of MGO would provide more negatively charged groups, thus creating new more sorption sites for positively charged Cd(II), resulting in slight enhancement of Cd(II) sorption capacity due to electrostatic attraction force at the initial Cd(II) concentration of 50 mg/L and 100 mg/L in Cd(II)–OG binary system. Therefore, the sorption capacity of Cd(II) onto MGO kept increase at the initial Cd(II) concentration of 300 mg/L in Cd(II)–OG binary system (displayed in Fig. 9), but decreased compared with that in mono-component system, leading to R value less than 1.

3.5. Desorption and reusability

Desorption behavior was studied using HCl solution and EG as eluants for Cd(II) and ionic dyes, respectively (displayed in Fig. 11). The value of cycle 0 was denoted as the adsorption of the original MGO. Results showed that adsorption capacities of Cd(II) and ionic dyes decreased with increasing regeneration cycle numbers. After the first regeneration cycle, the removal efficiencies were 67.55%, 55.76% and 83.01% for Cd(II), MB and OG, respectively. After the fourth cycle, the removal efficiencies were 33.78%, 42.25% and 47.32% for Cd(II), MB and OG, respectively, indicating that MGO adsorbent had the potential for reusability.

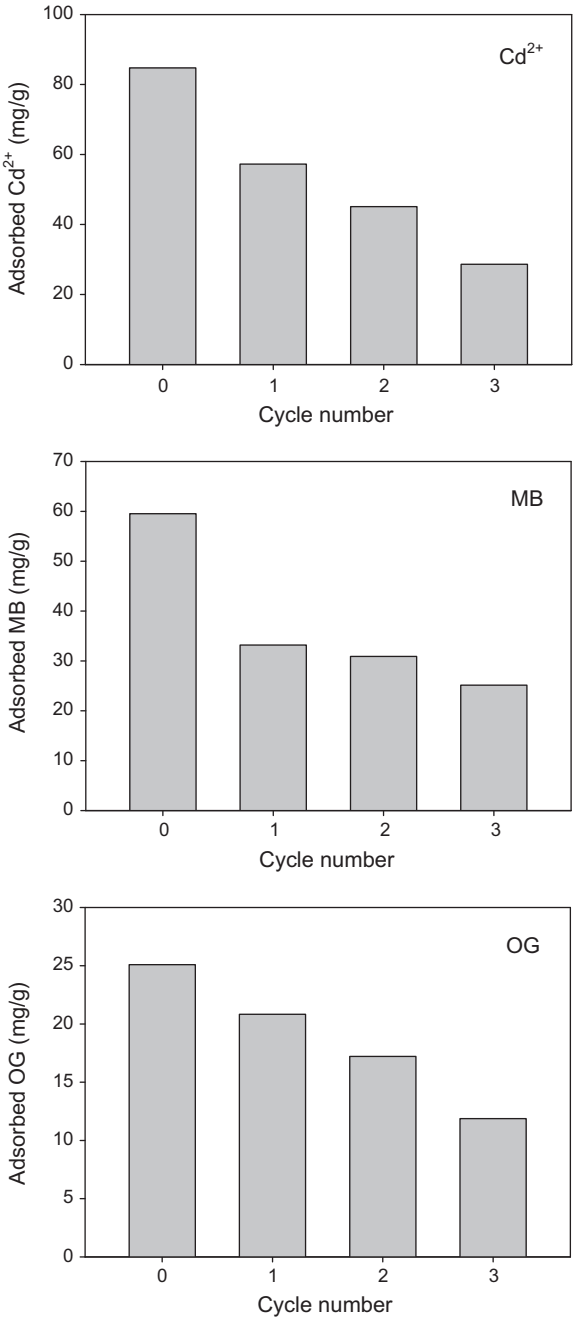

Fig. 11. Reusability of MGO in the removal of Cd(II), MB and OG. The initial concentrations of Cd(II), MB and OG were 500 mg/L, 120 mg/L and 150 mg/L. The adsorbent dosage was 1 g/L.

3.6. Application of MGO adsorbent in tap water

To evaluate the adsorbent performance of the MGO in real water samples, tap water samples spiked with dyes or Cd(II) were treated using the as-prepared MGO. The results showed that the maximum sorption capacities of MB, OG and Cd(II) onto MGO in tap water samples were 58.08 mg/g, 20.48 mg/g and 59.69 mg/g, respectively (shown in Fig. 12), which were 90.43%, 98.23% and 65.39% of those in ultrapure water. The decrease of sorption capacities of Cd(II) in tap water compared with that in ultrapure water may be caused by the increase of ionic strength in tap water. The sorption isotherms of MB, OG and Cd(II) onto MGO in tap water were better fitted with Langmuir model than Freundlich model (listed in Table 3). Noticeably, tap water samples had little interference with the performance of MGO toward MB and OG, suggesting that MGO adsorbent was suitable for removal of dyes from real water.

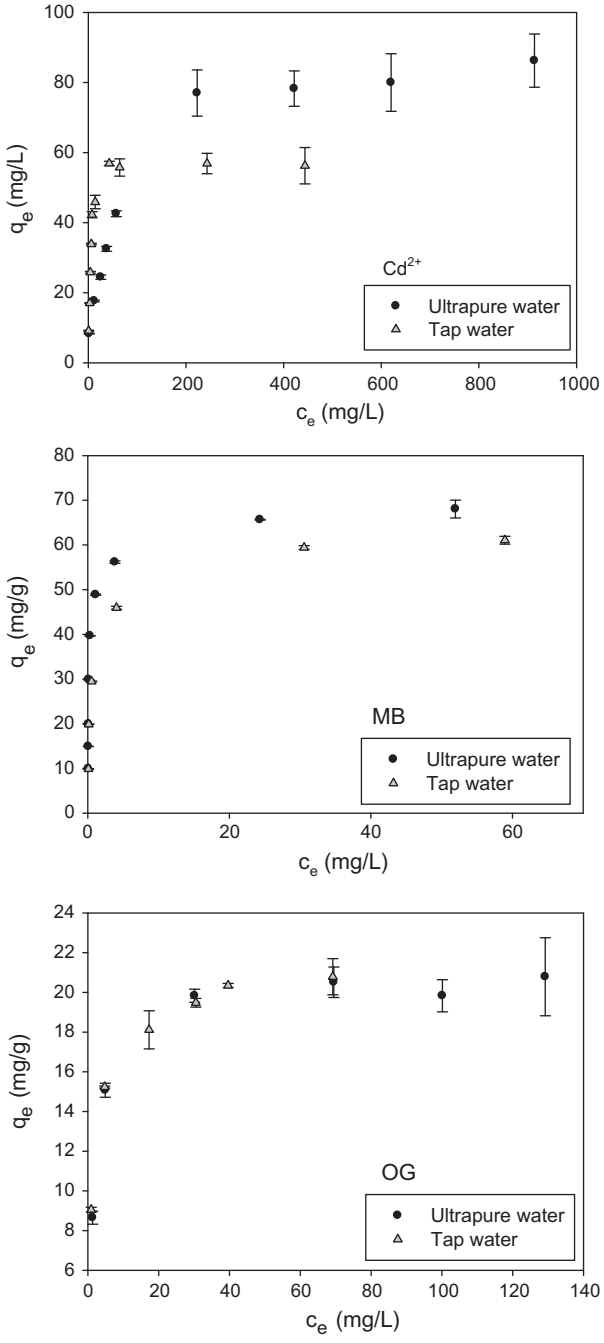

Fig. 12. Sorption curves for Cd(II), MB and OG onto MGO adsorbent in ultrapure and tap waters. pH = 6; contact time: 24 h; temperature, 25 °C; adsorbent dosage, 1 g/L.

4. Conclusions

In summary, MGO as an adsorbent was prepared for simultaneous removal of Cd(II) and ionic dyes including MB and OG. The sorption capacities increased for Cd(II) and MB and decreased for OG with increasing pH value. The sorption capacities increased sharply with time and the time required to reach the equilibrium was 165 min, 405 min and 405 min for Cd(II), MB and OG respectively. The sorption kinetics of dyes and Cd(II) were well described by pseudo second-order model. In mono-component system, the maximum sorption capacities in ultrapure water for Cd(II), MB and OG were 91.29 mg/g, 64.23 mg/g and 20.85 mg/g, respectively. The sorption capacity decreased for Cd(II) with increasing MB concentration and almost was not affected for MB with increasing Cd(II) concentration in Cd(II)–MB binary system. However, the sorption capacity of Cd(II) was independent on the OG concentration, but dependent on the initial Cd(II) concentration in Cd(II)–OG binary system. Noticeably, the sorption capacity of OG onto MGO enhanced with increasing Cd(II) concentration in Cd(II)–OG binary system. In tap water samples, the sorption capacity of Cd(II) was 65.39% of that in ultrapure water. However, the tap water samples had little interference with the performance of MGO toward MB and OG, indicating that MGO was suitable for removal of ionic dyes from real water.

Acknowledgements

The authors are grateful for the financial supports from National Natural Science Foundation of China (51039001, 50978088, 50808070, 51108166 and 51009063), the program for New Century Excellent Talents in University from the Ministry of Education of China (NCET-09-0328).

Appendix A. Supplementary material

Supplementary data associated with this article can be found, in the online version, at http://dx.doi.org/10.1016/j.cej.2013.04.045.

References

[1] C. Omeroglu Ay, A.S. Ozcan, Y. Erdogan, A. Ozcan, Characterization of Punica granatum L. peels and quantitatively determination of its biosorption behavior towards lead (II) ions and acid blue 40, Colloids Surf. B-Biointerfaces 100 (2012) 197–204.
[2] W. Ma, X. Song, Y. Pan, Z. Cheng, G. Xin, B. Wang, X. Wang, Adsorption behavior of crystal violet onto opal and reuse feasibility of opal-dye sludge for binding heavy metals from aqueous solutions, Chem. Eng. J. 193–194 (2012) 381–390.
[3] M.M.S. Saif, N.S. Kumar, M.N.V. Prasad, Binding of cadmium to strychnos potatorum seed proteins in aqueous solution: adsorption kinetics and relevance to water purification, Colloids Surf. B-Biointerfaces 94 (2012) 73–79.
[4] J. Zhu, S. Wei, H. Gu, S.B. Rapole, Q. Wang, Z. Luo, N. Haldolaarachchige, D.P. Young, Z. Guo, One-pot synthesis of magnetic graphene nanocomposites decorated with core@double-shell nanoparticles for fast chromium removal, Environ. Sci. Technol. 46 (2012) 977–985.
[5] P. Miretzky, A. Fernandez Cirelli, Cr(VI) and Cr(III) removal from aqueous solution by raw and modified lignocellulosic materials: a review, J. Hazard. Mater. 180 (2010) 1–19.
[6] Z. Pei, X.Q. Shan, J. Kong, B. Wen, G. Owens, Coadsorption of ciprofloxacin and Cu(II) on montmorillonite and kaolinite as affected by solution pH, Environ. Sci. Technol. 44 (2010) 915–920.
[7] Y. Masuda, M. Bekki, S. Sonezaki, T. Ohji, K. Kato, Dye adsorption characteristics of anatase TiO_2 film prepared in an aqueous solution, Thin Solid Films 518 (2009) 845–849.
[8] M.H. Karaoglu, M. Dogan, M. Alkan, Removal of reactive blue 221 by kaolinite from aqueous solutions, Ind. Eng. Chem. Res. 49 (2010) 1534–1540.

[9] T. Feng, F. Zhang, J. Wang, L. Wang, Application of chitosan-coated quartz sand for congo red adsorption from aqueous solution, J. Appl. Polym. Sci. 125 (2012) 1766–1772.
[10] M. Machida, B. Fotoohi, Y. Amamo, L. Mercier, Cadmium(II) and lead(II) adsorption onto hetero-atom functional mesoporous silica and activated carbon, Appl. Surf. Sci. 258 (2012) 7389–7394.
[11] R. Tovar-Gomez, D.A. Rivera-Ramirez, V. Hernandez-Montoya, A. Bonilla-Petriciolet, C.J. Duran-Valle, M.A. Montes-Moran, Synergic adsorption in the simultaneous removal of acid blue 25 and heavy metals from water using a $Ca(PO_3)_2$-modified carbon, J. Hazard. Mater. 199–200 (2012) 290–300.
[12] S.R. Shukla, R.S. Pai, Adsorption of Cu(II), Ni(II) and Zn(II) on dye loaded groundnut shells and sawdust, Sep. Purif. Technol. 43 (2005) 1–8.
[13] M. Visa, C. Bogatu, A. Duta, Simultaneous adsorption of dyes and heavy metals from multicomponent solutions using fly ash, Appl. Surf. Sci. 256 (2010) 5486–5491.
[14] C.L. Chen, X.K. Wang, M. Nagatsu, Europium adsorption on multiwall carbon nanotube/iron oxide magnetic composite in the presence of polyacrylic acid, Environ. Sci. Technol. 43 (2009) 2362–2367.
[15] M.A.A. Zaini, Y. Amano, M. Machida, Adsorption of heavy metals onto activated carbons derived from polyacrylonitrile fiber, J. Hazard. Mater. 180 (2010) 552–560.
[16] Q. Zhou, X. Wang, J. Liu, L. Zhang, Phosphorus removal from wastewater using nano-particulates of hydrated ferric oxide doped activated carbon fiber prepared by sol–gel method, Chem. Eng. J. 200–202 (2012) 619–626.
[17] S. Yang, J. Hu, C. Chen, D. Shao, X. Wang, Mutual effects of Pb(II) and humic acid adsorption on multiwalled carbon nanotubes/polyacrylamide composites from aqueous solutions, Environ. Sci. Technol. 45 (2011) 3621–3627.
[18] W.W. Tang, G.M. Zeng, J.L. Gong, Y. Liu, X.Y. Wang, Y.Y. Liu, Z.F. Liu, L. Chen, X.R. Zhang, D.Z. Tu, Simultaneous adsorption of atrazine and Cu(II) from wastewater by magnetic multi-walled carbon nanotube, Chem. Eng. J. 211–212 (2012) 470–478.
[19] S. Zhang, T. Shao, H. Selcen Kose, T. Karanfil, Adsorption of aromatic compounds by carbonaceous adsorbents: a comparative study on granular activated carbon, activated carbon fiber, and carbon nanotubes, Environ. Sci. Technol. 44 (2010) 6377–6383.
[20] G. Zhao, J. Li, X. Ren, C. Chen, X. Wang, Few-layered graphene oxide nanosheets as superior sorbents for heavy metal ion pollution management, Environ. Sci. Technol. 45 (2011) 10454–10462.
[21] G. Xie, P. Xi, H. Liu, F. Chen, L. Huang, Y. Shi, F. Hou, Z. Zeng, C. Shao, J. Wang, A facile chemical method to produce superparamagnetic graphene oxide–Fe_3O_4 hybrid composite and its application in the removal of dyes from aqueous solution, J. Mater. Chem. 22 (2012) 1033–1039.
[22] G. Zhao, T. Wen, C. Chen, X. Wang, Synthesis of graphene-based nanomaterials and their application in energy-related and environmental-related areas, RSC Adv. 2 (2012) 9286–9303.
[23] H. Sun, L. Cao, L. Lu, Magnetite/reduced graphene oxide nanocomposites: one step solvothermal synthesis and use as a novel platform for removal of dye pollutants, Nano Res. 4 (2011) 550–562.
[24] G. Zhao, L. Jiang, Y. He, J. Li, H. Dong, X. Wang, Sulfonated graphene for persistent aromatic pollutant management, Adv. Mater. 23 (2011) 3959–3963.
[25] W. Gao, M. Majumder, L.B. Alemany, T.N. Narayanan, M.A. Ibarra, B.K. Pradhan, P.M. Ajayan, Engineered graphite oxide materials for application in water purification, ACS Appl. Mater. Interfaces 3 (2011) 1821–1826.
[26] P. Bradder, S.K. Ling, S. Wang, S. Liu, Dye adsorption on layered graphite oxide, J. Chem, Eng. Data. 56 (2011) 138–141.
[27] W. Zhang, C. Zhou, W. Zhou, A. Lei, Q. Zhang, Q. Wan, B. Zou, Fast and considerable adsorption of methylene blue dye onto graphene oxide, Bull Environ. Contam. Toxicol. 87 (2011) 86–90.
[28] S. Yang, P. Zong, X. Ren, Q. Wang, X. Wang, Rapid and highly efficient preconcentration of Eu(III) by core–shell structured Fe_3O_4@humic acid magnetic nanoparticles, ACS Appl. Mater. Interfaces 4 (2012) 6891–6900.
[29] S. Bai, X. Shen, X. Zhong, Y. Liu, G. Zhu, X. Xu, K. Chen, One-pot solvothermal preparation of magnetic reduced graphene oxide–ferrite hybrids for organic dye removal, Carbon 50 (2012) 2337–2346.
[30] N. Li, M. Zheng, X. Chang, G. Ji, H. Lu, L. Xue, L. Pan, J. Cao, Preparation of magnetic $CoFe_2O_4$-functionalized graphene sheets via a facile hydrothermal method and their adsorption properties, J. Solid State Chem. 184 (2011) 953–958.
[31] K. Zhang, V. Dwivedi, C. Chi, J. Wu, Graphene oxide/ferric hydroxide composites for efficient arsenate removal from drinking water, J. Hazard. Mater. 182 (2010) 162–168.
[32] M. Liu, C. Chen, J. Hu, X. Wu, X. Wang, Synthesis of magnetite/graphene oxide composite and application for cobalt (II) remval, J. Phys. Chem. C 115 (2011) 25234–25240.
[33] V. Chandra, J. Park, Y. Chun, J.W. Lee, I.C. Hwang, K.S. Kim, Water-dispersible magnetite-reduced graphene oxide composites for arsenic removal, ACS Nano 4 (2010) 3979–3986.
[34] W.S. Hummers Jr., R.E. Offeman, Preparation of graphitic oxide, J. Am. Chem. Soc. 80 (1958) 1339.
[35] J.L. Gong, B. Wang, G.M. Zeng, C.P. Yang, C.G. Niu, Q.Y. Niu, W.J. Zhou, Y. Liang, Removal of cationic dyes from aqueous solution using magnetic multi-wall carbon nanotube nanocomposite as adsorbent, J. Hazard. Mater. 164 (2009) 1517–1522.
[36] M.A. Legodi, D. de Waal, The preparation of magnetite, goethite, hematite and maghemite of pigment quality from mill scale iron waste, Dyes Pigments 74 (2007) 161–168.
[37] X. Yang, C. Chen, J. Li, G. Zhao, X. Ren, X. Wang, Graphene oxide–iron oxide and reduced graphene oxide–iron oxide hybrid materials for the removal of organic and inorganic pollutants, RSC Adv. 2 (2012) 8821–8826.
[38] J.L. Gong, X.Y. Wang, G.M. Zeng, L. Chen, J.H. Deng, X.R. Zhang, Q.Y. Niu, Copper(II) removal by pectin–iron oxide magnetic nanocomposite adsorbent, Chem. Eng. J. 185–186 (2012) 100–107.
[39] T. Yamashita, P. Hayes, Analysis of XPS spectra of Fe^{2+} and Fe^{3+} ions in oxide materials, Appl. Surf. Sci. 254 (2008) 2441–2449.
[40] J.L. Gong, L. Chen, G.M. Zeng, F. Long, J.H. Deng, Q.Y. Niu, X. He, Shellac-coated iron oxide nanoparticles for removal of cadmium(II) ions from aqueous solution, J. Environ. Sci. 24 (2012) 1165–1173.
[41] Y.X. Chen, B.H. Zhong, W.M. Fang, Adsorption characterization of lead(II) and cadmium(II) on crosslinked carboxymethyl starch, J. Appl. Polym. Sci. 124 (2012) 5010–5020.
[42] Y. Feng, J.L. Gong, G.M. Zeng, Q.Y. Niu, H.Y. Zhang, C.G. Niu, J.H. Deng, M. Yan, Adsorption of Cd(II) and Zn(II) from aqueous solutions using magnetic hydroxyapatite nanoparticles as adsorbents, Chem. Eng. J. 162 (2010) 487–494.
[43] N. Benselka-Hadj Abdelkader, A. Bentouami, Z. Derriche, N. Bettahar, L.C. de Menorval, Synthesis and characterization of Mg–Fe layer double hydroxides and its application on adsorption of orange G from aqueous solution, Chem. Eng. J. 169 (2011) 231–238.
[44] R. Han, J. Zhang, P. Han, Y. Wang, Z. Zhao, M. Tang, Study of equilibrium, kinetic and thermodynamic parameters about methylene blue adsorption onto natural zeolite, Chem. Eng. J. 145 (2009) 496–504.
[45] T. Liu, Y. Li, Q. Du, J. Sun, Y. Jiao, G. Yang, Z. Wang, Y. Xia, W. Zhang, K. Wang, H. Zhu, D. Wu, Adsorption of methylene blue from aqueous solution by graphene, Colloids Surf. B-Biointerfaces 90 (2012) 197–203.
[46] G.K. Ramesha, A. Vijaya Kumara, H.B. Muralidhara, S. Sampath, Grphene and graphene oxide as effective adsorbents toward anionic and cationic dyes, J. Colloid Interf. Sci. 361 (2011) 270–277.
[47] D. Wu, P. Zheng, P.R. Chang, X. Ma, Preparation and characterization of magnetic rectorite/iron oxide nanocomposites and its application for the removal of the dyes, Chem. Eng. J. 174 (2011) 489–494.
[48] L. Ai, C. Zhang, Z. Chen, Removal of methylene blue from aqueous solution by a solvothermal-synthesized graphene/magnetite composite, J. Hazard. Mater. 192 (2011) 1515–1524.
[49] S. Qu, F. Huang, S. Yu, G. Chen, J. Kong, Magnetic removal of dyes from aqueous solution using multi-walled carbon nanotubes filled with Fe_2O_3 particles, J. Hazard. Mater. 160 (2008) 643–647.
[50] M. Arulkumar, P. Sathishkumar, T. Palvannan, Optimization of orange G dye adsorption by activated carbon of thespesia populnea pods using response surface methodology, J. Hazard. Mater. 186 (2011) 827–834.
[51] F. Ge, M.M. Li, H. Ye, B.X. Zhao, Effective removal of heavy metal ions Cd^{2+}, Zn^{2+}, Pb^{2+}, Cu^{2+} from aqueous solution by polymer-modified magnetic nanoparticles, J. Hazard. Mater. 211–212 (2012) 366–372.
[52] Y.J. Tu, C.F. You, C.K. Chang, Kinetics and thermodynamics of adsorption for Cd on green manufactured nano-particles, J. Hazard. Mater. 235–236 (2012) 116–122.
[53] M.A. Tofighy, T. Mohammadi, Adsorption of divalent heavy metal ions form water using carbon nanotube sheets, J. Hazard. Mater. 185 (2011) 140–147.